A New Sensorless Speed Control Scheme for Doubly Fed Reluctance Generators

Sul Ademi, *Member, IEEE*, Milutin G. Jovanović, *Senior Member, IEEE*, Hamza Chaal, and Wenping Cao, *Senior Member, IEEE*

***Abstract*—This paper presents the development and experimental validation of a novel angular velocity observer-based field-oriented control algorithm for a promising low-cost brushless doubly fed reluctance generator (BDFRG) in wind power applications. The BDFRG has been receiving increasing attention because of the use of partially rated power electronics, the high reliability of brushless design, and competitive performance to its popular slip-ring counterpart, the doubly fed induction generator. The controller viability has been demonstrated on a BDFRG laboratory test facility for emulation of variable speed and loading conditions of wind turbines or pump drives.**

***Index Terms*—Angular velocity control, brushless machines, reactive power control, sensorless control, wind energy generation.**

I. Introduction

BRUSHLESS doubly-fed generators (BDFGs) [1]–[5] have been considered as a possible alternative to traditional doubly-fed induction generators (DFIGs) [6] for wind energy conversion systems (WECS) with limited speed ranges. As members of the same slip power recovery family, both the machines share the cost benefits of a proportionally smaller inverter being usually around 30% of their rating [6], [7]. These advantages over bulky and expensive multi-pole synchronous generators (SGs) with fully-rated power converters [6] featuring higher failure rates [8], are accompanied by the well-known DFIG reliability issues of brush gear, which entails regular maintenance and may be an obstacle for its long-term use [8], [9]. This concern for DFIG's future has been further reinforced with the introduction of the national grid codes and strict regulations for the low-voltage-fault-ride-through (LVFRT) performance [6], giving preference to wound rotor or permanent magnet SGs [8], the DFIG's main competitor on the wind power market [6], [8].

The BDFG may be a solution to overcome the above DFIG drawbacks and medium-scale prototypes have been recently built [10] with large 2 MW designs proposed [3], [5]. As the name implies, brushes and slip rings are eradicated, hence the more reliable and maintenance-free operation. These favorable properties should be appealing for off-shore wind turbines [2], [3], where the DFIG running costs can be substantial [8], [9]. Another essential BDFG merit is the distinguishing LVFRT capability, which can be accomplished safely without crowbar circuitry [4] owing to the relatively higher leakage inductances and lower fault current levels compared to the DFIG [11], [12].

The contemporary BDFG comprises two ordinary, sinusoidally distributed three-phase stator windings of generally different applied frequencies and pole numbers, with a rotor having half the total number of stator poles to produce the shaft position dependent magnetic coupling between the windings for the torque production [13]. The primary is connected to the mains, while the secondary (control) winding is normally supplied through a fractional dual-bridge converter in "back-to-back" configuration to allow bi-directional power flow (see Fig. 1). The rotor can take a modern reluctance form (e.g., BDFRG in Fig. 1) [14] or a special "nested" cage structure (e.g., BDFIG) [15]. Other, less common wound rotor BDFIG types [16]–[19] or BDFRG designs [20] are also feasible. By the absence of the rotor windings, the BDFRG should offer the higher efficiency [21] with simpler dynamic modeling [22] and inherently decoupled field-oriented control (FOC) of primary real and reactive power [1], [2], [23], in contrast to the BDFIG [15], [24]–[26]. The emphasis of this paper therefore contemplates on the BDFRG as a prominent forthcoming technology.

Similar studies to those conducted for the BDFIG [24]–[26] or DFIG [6] have also been done on the BDFRG(M) involving: scalar control [2], [23], vector control (VC) [1], [2], [5], [23], [27]–[29], direct torque and secondary flux (λ_s) [23], [30] or primary reactive power (Q) control (DTC) [31], direct power control [32] and variable structure control [33]. The preliminary attributes in [2], [23] and [33] are intellectually interesting but have been left unproven in practice. On the other hand, an original model-based DTC approach put forward in [30] has been experimentally substantiated with, and in [23] without, a shaft position sensor for speed regulation. However, the DTC methodologies in [23] and[30] are extremely sensitive to inductance knowledge and λ_s estimation inaccuracies so that poor proof of concept results for an unloaded BDFRM have just been reported. These shortcomings have been eliminated and much better response provided by replacing λ_s with Q as a control variable in the improved parameter independent DT(P)C schemes [31], [32] albeit at fixed BDFRG(M) loads of no or little interest to the target applications. Although robust and relatively easy to implement in a stator frame without having to

Manuscript received July 4, 2015; revised November 6, 2015; accepted December 14, 2015. Paper no. TEC-00475-2015.

S. Ademi is with the Department of Electronic and Electrical Engineering, Institute for Energy and Environment, University of Strathclyde, Glasgow G1 1RD, U.K. (e-mail: sul.ademi@strath.ac.uk).

M. Jovanović is with the Faculty of Engineering and Environment, Department of Physics and Electrical Engineering, Northumbria University, Newcastle upon Tyne NE1 8ST, U.K. (e-mail: milutin.jovanovic@northumbria.ac.uk).

H. Chaal is with the Renewable Energy Division, Siemens, plc., Keele ST5 5NP, U.K. (e-mail: hamza.chaal@siemens.com).

W. Cao is with the School of Engineering and Applied Science, Aston University, Birmingham B4 7ET, U.K. (e-mail: w.p.cao@aston.ac.uk).

Color versions of one or more of the figures in this paper are available online at http://ieeexplore.ieee.org.

Digital Object Identifier 10.1109/TEC.2016.2533609

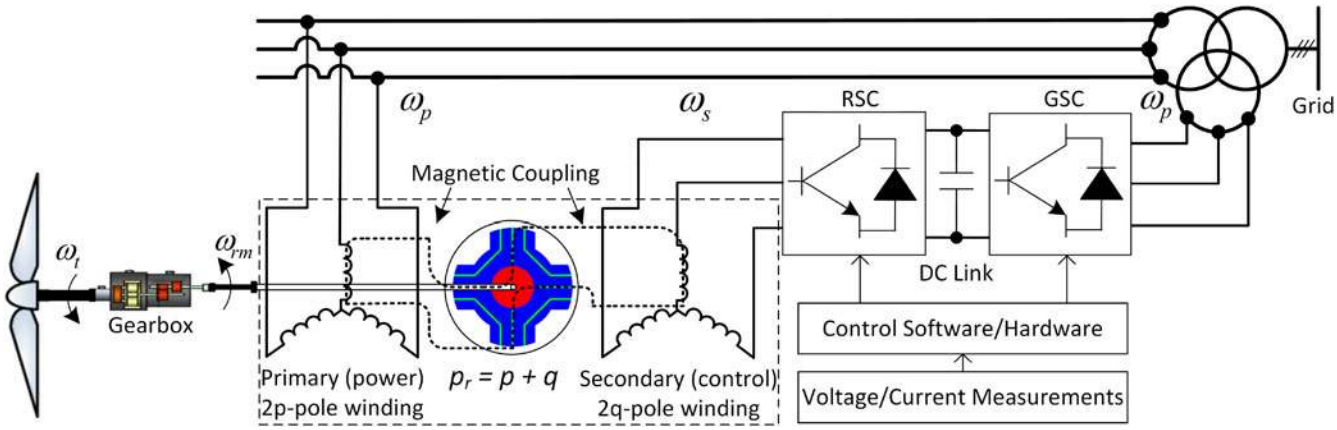

Fig. 1. A conceptual diagram of the BDFRG based WECS.

know the rotor position or speed, the hysteresis torque (power) controllers in [31] and [32] suffer from usual variable switching frequencies and higher flux (torque) ripples, unlike, in this sense, the undoubtedly superior VC. Besides, an encoder is solely required for speed regulation in [31] and [32], and its use is under-utilized from this point of view compared to the VC where it additionally serves for torque control.

VC with voltage (VOC) or flux (field) space-vector orientation (FOC) has been a widely adopted option in both industrial and academic circles for vast majority of adjustable speed drive and generator systems, including WECS. As such, it has been intensively investigated for commercial DFIGs or SGs [6] as well as the emerging BDFIG [24]–[26] and BDFRG [1], [2], [5], [23], [27]–[29], [34] substitutes. A VOC algorithm for motoring (BDFRM) and generating (BDFRG) regimes of the machine has been firstly proposed, simulated and implemented in [1]. Despite the apparent significance of this contribution, the introductory test results for variable speed operation of an unloaded BDFRM have only been produced. The theoretical considerations of the VC concept in [2] and [23] have not been supported by true measurements. Further efforts and important practical advances have been made in [27]–[29] with a comparative performance analysis of the two robust VOC and FOC methods for the small BDFRM [27] and the BDFRG [28], [29], [34] under both speed independent [28], [34] and variable loading conditions [27], [29], [34]. Similar, but computer simulation, VC studies for a 2 MW BDFRG wind turbine have been published in [5].

The BDFG works referenced above almost exclusively rely on the rotor position information for closed-loop speed control. Sensorless operation is desirable as shaft encoders bring many limitations in terms of cost, maintenance, sturdiness, and cabling requirements [6]. The latter deficiency may be particularly severe with DFIG turbines where regular brush servicing can pose a growing risk of sensor failure judging by the recent field statistics [8], [9]. This fact has largely motivated the overwhelming research on sensorless control of DFIG, a thorough review of which can be found in [6], [35]–[39]. The model complexities and heavy parameter dependence are the most likely reasons for the lack of publications on this subject for the BDFIG [15], [40]. Except for [23] on DTC, to the best of the authors' knowledge, there is no other journal article published on sensorless speed control in the BDFRG(M) literature to date either. This paper should partly fill the existing void by presenting the main idea, design aspects and experimental verification of a new rotor position estimation technique for encoder-less FOC of the BDFRG.

II. BDFRG Fundamentals

The focal angular velocity relationship for the electromechanical energy conversion in the BDFRG is [2], [22]:

$$\omega_{rm} = \frac{\omega_p + \omega_s}{p_r} = \frac{\omega_p}{p_r} \cdot \left(1 + \frac{\omega_s}{\omega_p}\right) = \omega_{syn} \cdot \left(1 + \frac{\omega_s}{\omega_p}\right) \tag{1}$$

where $\omega_{syn} = \omega_p / p_r$ is obtained for $\omega_s = 0$, i.e., a dc secondary as with a $2p_r$-pole wound field synchronous turbo-machine. Notice that $\omega_s > 0$ for "super-synchronous" operation, and $\omega_s < 0$ (e.g., an opposite phase sequence of the secondary to the primary winding) in "sub-synchronous" mode.

Using (1), the mechanical power balance showing individual contributions of each machine winding, assuming *motoring* (BDFRM) convention as default, can be written as:

$$P_m = T_e \cdot \omega_{rm} = \underbrace{\frac{T_e \cdot \omega_p}{p_r}}_{P_p} + \underbrace{\frac{T_e \cdot \omega_s}{p_r}}_{P_s} = P_s \cdot \left(1 + \frac{\omega_p}{\omega_s}\right) \tag{2}$$

In the BDFRG case, $T_e < 0$ and thus $P_p < 0$, implying that positive power is fed to the grid by the primary winding, while the secondary power (P_s) flow can be bi-directional subject to the operating speed region.

III. D-Q Modeling Principles

The BDFRM steady-state model in a $d_p - q_p$ frame for the ω_p rotating primary winding space-vectors, and a $d_s - q_s$ frame for the ω_s rotating secondary counterparts (see Fig. 2), can be

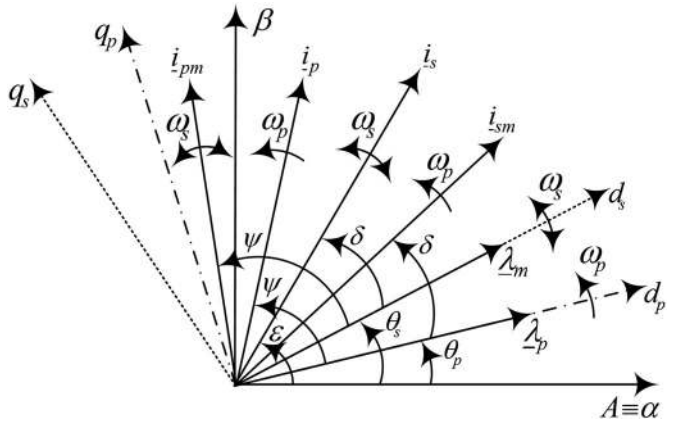

Fig. 2. Angular positions of the characteristic space-vectors in the respective rotating reference frames under FOC scenario.

represented as [2], [22]:

$$\left.\begin{aligned}
\underline{v}_p &= R_p \underline{i}_p + \frac{d\underline{\lambda}_p}{dt} = R_p \underline{i}_p + j\omega_p \underline{\lambda}_p \\
\underline{v}_s &= R_s \underline{i}_s + \frac{d\underline{\lambda}_s}{dt} = R_s \underline{i}_s + j\omega_s \underline{\lambda}_s \\
\underline{\lambda}_p &= L_p \underbrace{(i_{pd} + j i_{pq})}_{\underline{i}_p} + L_m \underbrace{(i_{sm_d} - j i_{sm_q})}_{\underline{i}^*_{sm}} \\
\underline{\lambda}_s &= L_s \underbrace{(i_{sd} + j i_{sq})}_{\underline{i}_s} + L_m \underbrace{(i_{pm_d} - j i_{pm_q})}_{\underline{i}^*_{pm}}
\end{aligned}\right\} \tag{3}$$

The flux equations of (3) can be manipulated as [2], [23]:

$$\underline{\lambda}_p = \underbrace{L_p i_{pd} + L_m i_{sm_d}}_{\lambda_{pd}} + j \cdot \underbrace{(L_p i_{pq} - L_m i_{sm_q})}_{\lambda_{pq}} \tag{4}$$

$$\underline{\lambda}_s = \underbrace{\sigma L_s i_{sd} + \lambda_{md}}_{\lambda_{sd}} + j \cdot \underbrace{(\sigma L_s i_{sq} + \lambda_{mq})}_{\lambda_{sq}} = \sigma L_s \underline{i}_s + \underbrace{\frac{L_m}{L_p} \underline{\lambda}^*_p}_{\underline{\lambda}_m} \tag{5}$$

where λ_m is the primary flux coupling the secondary winding (i.e., the mutual flux linkage), $L_{p,s,m}$ are the three-phase self and mutual inductances [2], [22], $\underline{i}_{sm}$ is the magnetically coupled (magnetizing) secondary current vector ($\underline{i}_s$) of the same magnitude but modulated frequency (i.e., $\underline{i}_{sm} = \underline{i}_s$ in the respective frames), and vice-versa for $\underline{i}_{pm} = \underline{i}_p$ as indicated in Fig. 2. It should be stressed here that $\underline{i}_{sm}$, $\underline{i}_p$ and $\underline{\lambda}_p$ in (3) and (4) are in ω_p frame, whereas $\underline{i}_s$, $\underline{i}_{pm}$ and $\underline{\lambda}_m$ in (3) and (5) are in $p_r\omega_{rm} - \omega_p = \omega_s$ frame according to (1). This frame selection is termed as "natural" since the corresponding dq vector components become dc quantities, which are easier to control. The remaining dynamic modeling and operating peculiarities of the BDFRG(M) are explained in detail in [22]. The previous current vector equalities and (1) are key for the development of the rotor position estimation technique and the entire sensorless speed control algorithm in the sequel.

IV. FOC Conditions

Setting $\lambda_{pq} = 0$ and $\lambda_{mq} = 0$ (e.g., with the d_p-axis aligned to $\underline{\lambda}_p$ as in Fig. 2), and substituting (4) into $P_p + jQ_p = \frac{3}{2} j\omega_p \underline{\lambda}_p \underline{i}^*_p$, one can derive the following equivalent FOC expressions for torque and reactive power [27], [28]:

$$T_e = \frac{P_p p_r}{\omega_p} = \frac{3p_r}{2}\lambda_p i_{pq} = \frac{3p_r L_m}{2L_p}\lambda_p i_{sq} = \frac{3p_r}{2}\lambda_m i_{sq} \tag{6}$$

$$Q_p = \frac{3}{2}\omega_p \lambda_p i_{pd} = \frac{3}{2}\frac{\omega_p \lambda_p}{L_p}(\lambda_p - L_m i_{sd}) \tag{7}$$

A noteworthy remark from Fig. 2 is that if the d_p-axis lies along the $\underline{\lambda}_p$, then the complementary d_s-axis of the secondary (control) frame gets automatically aligned to $\underline{\lambda}_m$. Such a frame-flux vector mapping is intrinsic with the FOC and brings the benefits of inherently decoupled control of T_e (or P_p) and Q_p through i_{sq} and i_{sd} variations, respectively, as follows from (6) and (7). However, this significant advantage over VOC [27], [28] comes at the cost of the $\underline{\lambda}_p$ angle estimation (θ_p in Fig. 2). The R_p knowledge is also required for enhanced performance with decreasing machine sizes [27], [28], but is rather obsolete at large-scale level [3] where R_p is negligible making the FOC virtually parameter independent [5]. It has been experimentally shown in [27] and[28] that the VOC without cross-coupling compensation has a much worse load disturbance rejection ability as a trade-off of the entire parameter freedom. The FOC approach has been therefore chosen for implementation as illustrated in Fig. 3.

Note that with the approximately constant λ_p, and thus λ_m, magnitudes by the primary winding grid connection, (6) and (7) are nearly linear relationships, which vindicates the use of i^*_{sq} (instead of usual T^*_e) and i^*_{sd} as reference outputs of the respective speed and Q loops subject to the control selector position (see Fig. 3). Doing so, the unknown parameter variations are effectively taken care of by appropriately tuning the PI gains. The control in Fig. 3 is completely carried out without an encoder as described in the following section.

V. Sensorless Control Procedure

The primary flux vector constituents in a stationary $\alpha - \beta$ frame (see Fig. 2) are derived from the measured phase voltages and currents in a fairly standard manner using (3):

$$\underline{\lambda}_{\alpha\beta} = \lambda_p e^{j\theta_p} = \lambda_\alpha + j\lambda_\beta = \int (\underline{v}_{\alpha\beta} - R_p \underline{i}_{\alpha\beta}) dt \tag{8}$$

where for a Y-connected winding with an isolated neutral point and "ABC" phase sequence:

$$\left.\begin{aligned}
&i_\alpha = i_A, i_\beta = (i_A + 2i_B)/\sqrt{3} \\
&v_\alpha = (2v_A - v_B - v_C)/3, v_\beta = (v_B - v_C)/\sqrt{3}
\end{aligned}\right\} \tag{9}$$

Advantages of using (8), which in digital form appears in Fig. 3, are two-fold: (i) The switching ripple-free line voltage waveforms of fixed magnitude and frequency (ω_p); (ii) Negligible λ_p and θ_p estimation errors due to the R_p temperature variations from the measured "cold" dc value used for calculations at full supply voltage. The obtained $\lambda_{\alpha\beta}$ estimates are

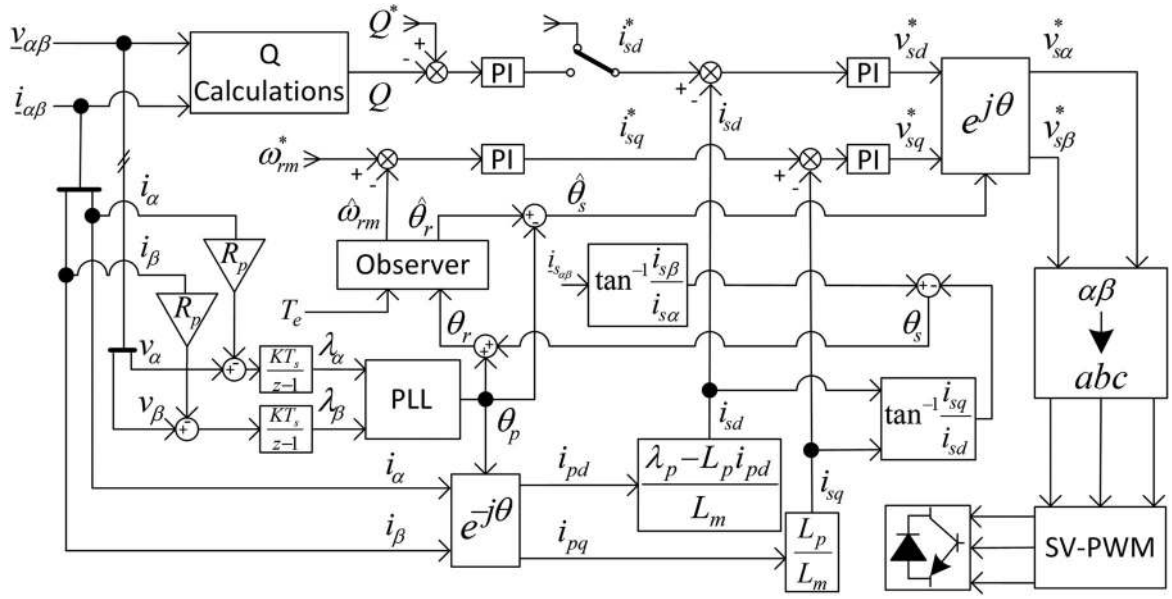

Fig. 3. A structural block diagram of the proposed speed sensorless FOC for the inverter-fed BDFRG with space-vector-PWM.

processed through a conventional phase-locked-loop filter [41] to suppress the usual effects of transducer dc offset and noise in measurements. The "cleaned" θ_p is employed to find the $d_p - q_p$ currents, i_{pd} and i_{pq}, by applying the well-known frame transformations as shown in Fig. 3, and to identify the rotor angle (θ_r) from the angular position version of (1) [22]:

$$\omega_r = p_r \omega_{rm} = \omega_p + \omega_s \Leftrightarrow \theta_r = p_r \theta_{rm} = \theta_p + \theta_s \tag{10}$$

The determination of the d_s-axis position (θ_s) in (10) is, however, far less transparent. The FOC forms of (4) and (8) are used as a starting point in this direction bearing in mind that $\underline{i}_{sm} = \underline{i}_s$ (see Section III and Fig. 2):

$$\lambda_{pd} = \lambda_p = L_p i_{pd} + L_m \underbrace{i_{sm_d}}_{=i_{sd}} \Longrightarrow i_{sd} = \frac{\lambda_p - L_p i_{pd}}{L_m} \tag{11}$$

$$\lambda_{pq} = 0 = L_p i_{pq} - L_m \underbrace{i_{sm_q}}_{=i_{sq}} \Longrightarrow i_{sq} = \frac{L_p}{L_m} i_{pq} \tag{12}$$

One should point out that the above relationships immediately define the control feedback currents (see Fig. 3) irrespective of θ_s or θ_r errors. Another benefit is that they allow θ_s to be worked out from measurements using (9) as a difference between the $\underline{i}_s$ angles in the stationary and rotating frames (see Fig. 2). The initial expressions applied for this purpose (see Fig. 3) are further expanded below using (11) and (12) as:

$$\theta_s = \underbrace{\operatorname{atan}\frac{i_{s\beta}}{i_{s\alpha}}}_{\varepsilon} - \underbrace{\operatorname{atan}\frac{i_{sq}}{i_{sd}}}_{\delta} = \underbrace{\operatorname{atan}\frac{i_a + 2i_b}{\sqrt{3} i_a}}_{\varepsilon} - \underbrace{\operatorname{atan}\frac{L_p i_{pq}}{\lambda_p - L_p i_{pd}}}_{\delta} \tag{13}$$

An important insight from (13) is the light parameter dependence of θ_s estimation as only L_p needs to be known in addition to R_p (through λ_p) with smaller machines. Nevertheless, as θ_s is still susceptible to measurement noise and numerical sensitivity to other uncertainties, the raw θ_r values coming from the solution of (10) are input to a common closed-loop PI observer (see Fig. 4) [42] to filter out erroneous estimates and accurately predict $\hat{\omega}_{rm}$. The enhanced $\hat{\theta}_r$ is then fed back into (10) to generate purified $\hat{\theta}_s$ signals and improve the quality of the resulting pulse width modulation (PWM) waveforms. These corrective actions are imperative to achieve the smooth controller response.

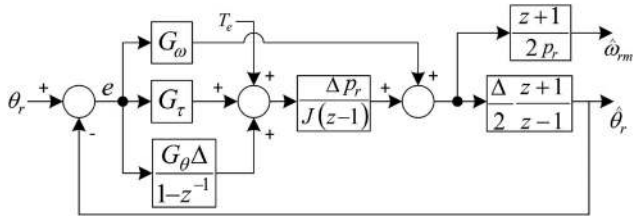

Fig. 4. A discrete load model based rotor angular velocity observer design.

TABLE I
THE BDFRG PARAMETERS AND RATINGS

Rotor inertia $[J]$	0.2 kg · m^2
Primary resistance $[R_p]$	11.1 Ω
Secondary resistance $[R_s]$	13.5 Ω
Primary inductance $[L_p]$	0.41 H
Secondary inductance $[L_s]$	0.57 H
Mutual inductance $[L_m]$	0.34 H
Rotor poles $[p_r]$	4
Primary power $[P_r]$	1.6 kW
Rated speed $[n_r]$	950 rev/min
Stator currents $[I_{p,s}]$	2.5 A rms
Stator voltage $[V_p]$	400 V rms
Stator frequency $[f_p]$	50 Hz
Winding connections	Y/Y
Stator poles $[p/q]$	6/2

However, apart from L_p, the magnetizing inductance (L_m) is also required for calculating the feedback current components, i_{sd} and i_{sq}, as shown in Fig. 3. The values in Table I, identified by off-line testing as described in [21], were used for this purpose. Careful tuning of current controller PI gains was deemed

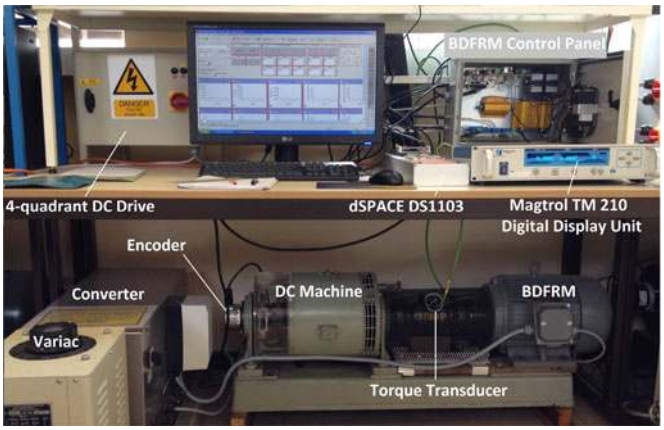

Fig. 5. A photo of the BDFRG laboratory test facility for WECS emulation.

necessary to minimise the harmful effects of machine model and/or inductance knowledge inaccuracies and noise in measurements on the control performance. In this sense, the proposed sensorless method, although more practical for larger machines [6], would be less robust to parameter variations than the high-frequency signal injection counterparts applied to DFIG [35], [39], but not yet developed for the BDFRG.

The primary winding P and Q calculations for control or monitoring (in this paper) have been done using (9) and:

$$\left.\begin{aligned} P &= \frac{3}{2}(i_\alpha \cdot v_\alpha + i_\beta \cdot v_\beta) \\ Q &= \frac{3}{2}(i_\alpha \cdot v_\beta - i_\beta \cdot v_\alpha) \end{aligned}\right\} \tag{14}$$

Considering that the power is a reference frame invariant quantity, this is deduced to be the least computationally intensive approach as unnecessary frame conversions of $v_{\alpha\beta}$ and $i_{\alpha\beta}$ can be eluded with the higher control rates achievable. The Q reference is often set to zero ($Q^* = 0$) for the unity line power factor, but it can be used to optimize any other performance measure for a given ω^*_{rm} in Fig. 3, usually corresponding to the MPPT of a wind turbine [2], [6].

A. Rotor Angular Velocity and Position Observer

The observer in Fig. 4 [42] has been devised from the conventional mechanical equations for the machine ignoring friction, which are reproduced here for convenience:

$$\left.\begin{aligned} J\frac{d\omega_r}{dt} &= p_r(T_e - T_L) \\ \omega_r &= \frac{d\theta_r}{dt} = p_r\omega_{rm} \end{aligned}\right\} \tag{15}$$

where J is the inertia constant (see Table I) of the BDFRG-prime mover combination (see Fig. 5), which was precisely obtained by applying a standard step-torque test [21].

The merit of using an observer is that both $\hat{\omega}_{rm}$ and $\hat{\theta}_r$ can be predicted without any knowledge of past information, and therefore with no phase lag which is crucial for high performance control. The digital form of the filter is implemented using an optimal sequence of forward and backward approximations for the three integrators so that the delay through the algorithm is reduced to a minimum. This type of observer is preferable to either classical filtering or recursive estimation approaches for drive and generator applications [43], [44]. For position sensor based control strategies, the input into the observer is fairly precise, so the gains G_ω, G_τ and G_θ should be larger to ensure fast convergence to the measured θ_r. A high accuracy, insensitivity to both model and load parameter (J) errors, and compensation for the state disturbances caused by load torque T_L can be accomplished by means of the $\hat{\theta}_r$ feedback and position error integrator.

However, in case of the sensorless control, the response rate of the observer has to be compromised to some extent to account for the noisy θ_r produced by the position estimator. The convergence of the control algorithm and machine operating stability are simply a matter of appropriately tuning the observer gains, the main criteria being the quality of θ_r. If the estimates are known to be good then the feedback gain is increased, else it is decreased. This implies that gain scheduling may be required to get good estimates over the entire speed range. In our experiments, θ_r values were mostly accurate enough so the fixed gains could be used throughout. The latter were tuned heuristically by "trial and error" method.

VI. BDFRG Wind Turbine Emulation

A geared horizontal-axis wind turbine is typically operated in a variable speed range of 2:1 or so. For the 6/2-pole BDFRG being investigated, this is [950, 550] rev/min, i.e., 200 rev/min around synchronous speed for a $f_p = 50$ Hz supply. The speed limits are achieved at the boundary secondary frequencies of $f_s \approx \mp 0.27 \cdot f_p \approx 13$ Hz given (1). It could be easily shown using (2) that $P_s \approx 0.21\, P_m$ meaning that the inverter would have to handle at most 21% of the mechanical power (plus total losses on the secondary side) in this case.

The turbine torque driving the generator for the maximum wind energy extraction in the base speed region (i.e., between "cut-in" and rated wind speed) can be represented as [2], [6]:

$$T_{mppt} = C_{mppt} \cdot \omega^2_{rm} \tag{16}$$

where the C_{mppt} constant is a function of the turbine parameters for the MPPT operation at the optimum tip-speed ratio.

The BDFRG data from Table I were identified by off-line testing by applying the methods described in [21]. These BDFRG specifications have served to tailor a suitable torque-speed profile of the same form as (16):

$$T_L = -\frac{P_r}{\omega_r} \cdot \left(\frac{n_{rm}}{n_r}\right)^2 \approx -16 \cdot \left(\frac{n_{rm}}{950}\right)^2 \text{N·m} \tag{17}$$

The above expression is implemented to emulate the wind turbine characteristics using an off-the-shelf motor equipped with a commercial dc drive operated in torque mode (see Fig. 5).

VII. Experimental Results

The results in Figs. 6–9 have been produced by executing the sensorless scheme in Fig. 3 on a Simulink compatible dSPACE

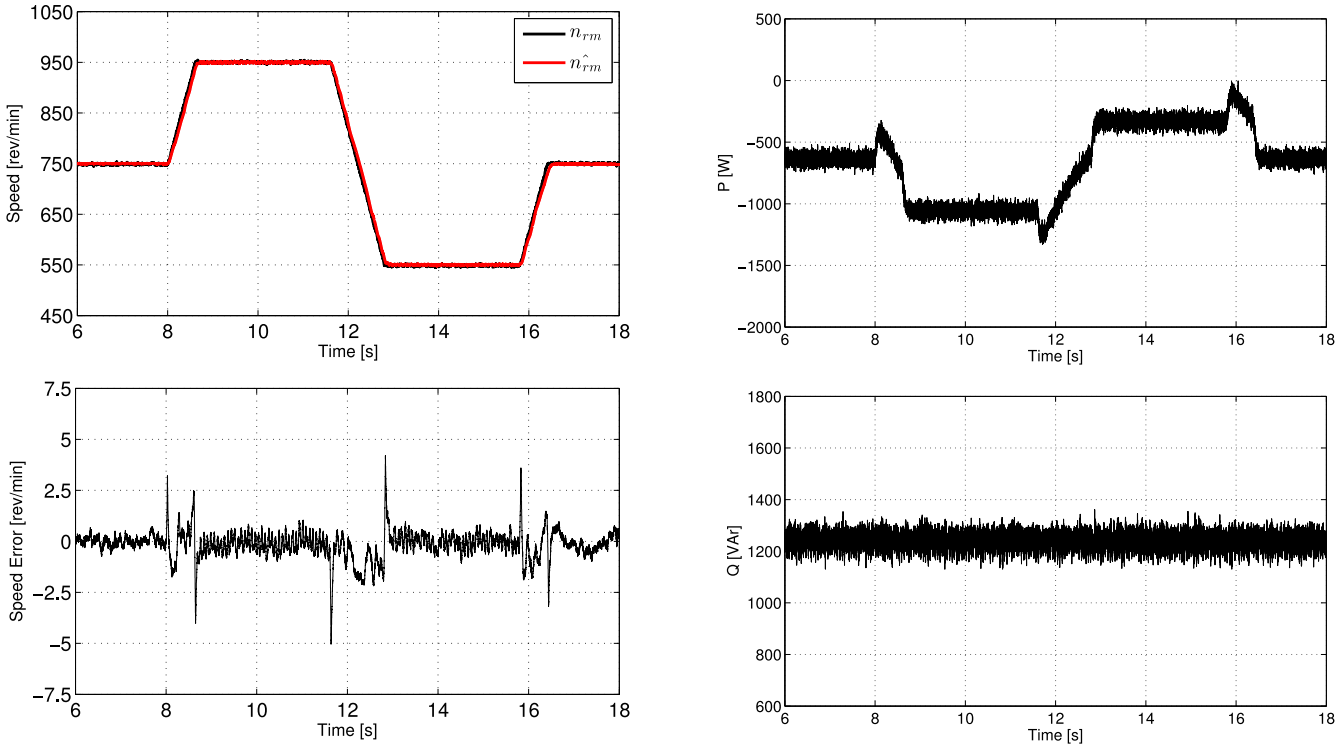

Fig. 6. Experimental verification of the BDFRG sensorless speed control: actual, estimated speed and estimation errors (left); real and reactive power (right).

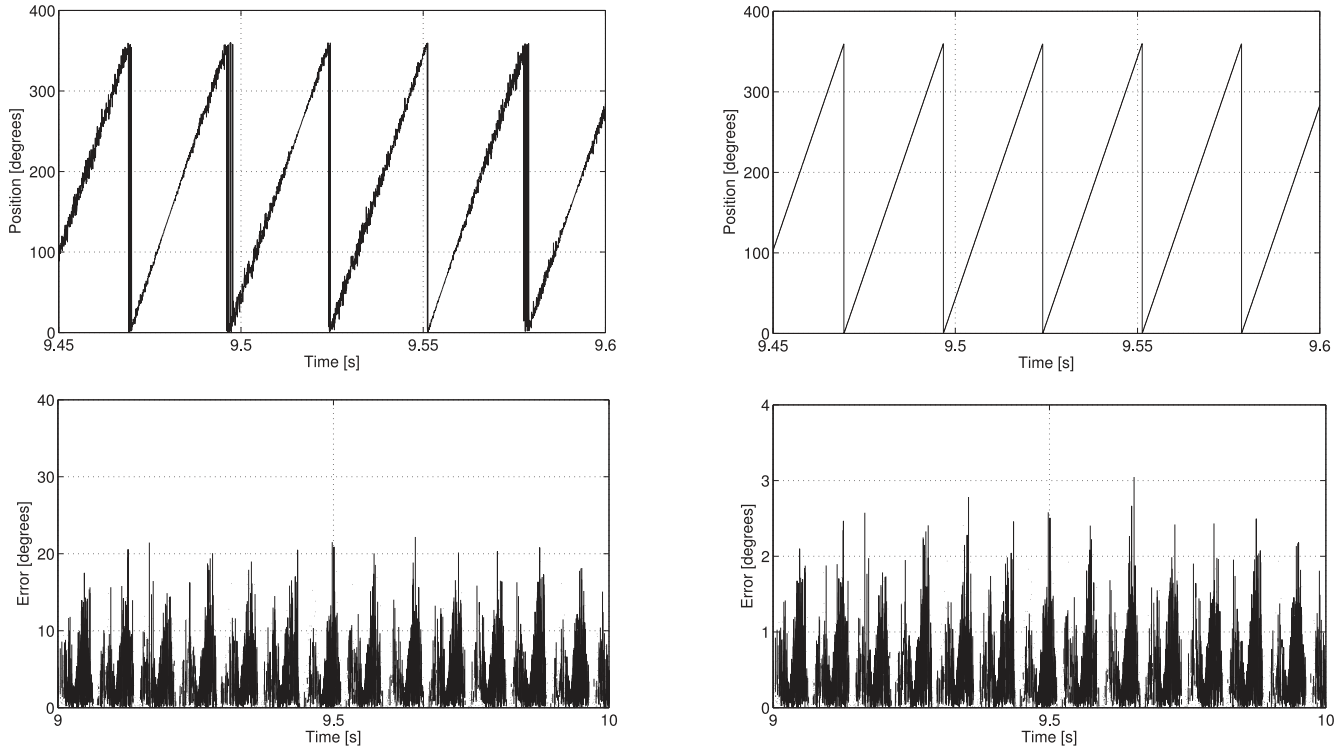

Fig. 7. Estimated rotor position angles and respective absolute estimation errors at 950 rev/min before (left) and after (right) passing through the observer.

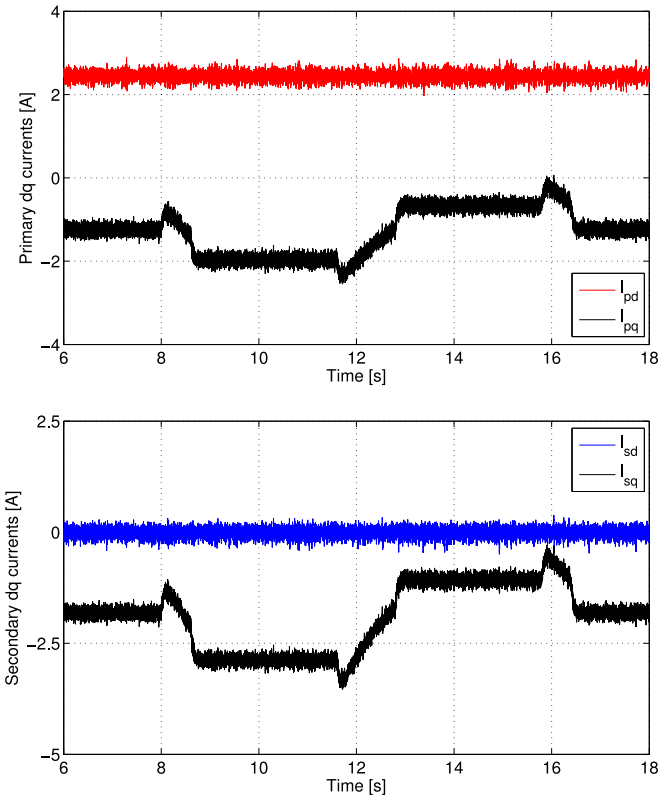

Fig. 8. MTPIA performance of the BDFRG with sensorless speed control.

platform (see Fig. 5) at 2.5 kHz PWM switching rate using the maximum torque per inverter ampere (MTPIA) strategy (i.e., by setting $i^*_{sd} = 0$) [2]. The MTPIA objective has been selected in order to achieve the minimum current loading on the BDFRG secondary side, and hence reduction of both the copper and converter losses, for a given torque. The line power factor would be inevitably compromised in this case by the entirely magnetizing nature of the primary winding with the torque producing secondary currents.

The two left-column graphs in Fig. 6 demonstrate a precise sensorless tracking of synchronous (750 rev/min), sub-synchronous (550 rev/min) and super-synchronous (950 rev/min) speeds with very little estimation errors for a random cyclically varying steep ramp signal, dynamically suited to WECS even at extreme turbulent winds. Notice that the Q behavior is essentially unaffected by the P variations at any speed clearly indicating the inherently decoupled FOC nature as previously anticipated by (6) and (7).

The left-hand plots in Fig. 7 represent the rotor angles (θ_r), obtained from (10) for θ_s given by (13), and their absolute deviations from encoder measurements. Note that a shaft position sensor in Fig. 5 was only used for instrumentation purposes and not for control. The raw θ_r estimates are notably spiky, but despite the errors occasionally peaking over 20°, the mean value is still reasonably low (≈6°). These sporadic excursions of the estimation errors are mainly caused by the practical effects of measurement noise and transducer quantization at relatively lower MTPIA secondary current magnitudes.

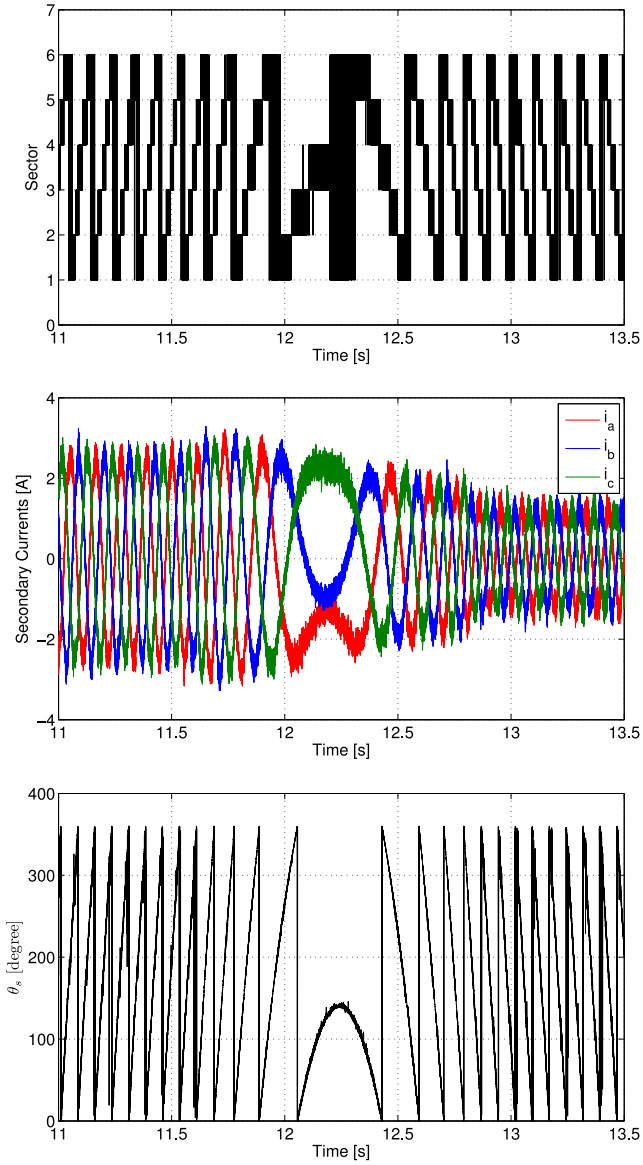

Fig. 9. Experimental results for the inferred secondary voltage positions and measured secondary current waveforms showing a phase sequence reversal during the transition from super to sub-synchronous speed.

The observer capacity as a low-pass filter is evident from Fig. 7, and a considerable improvement in accuracy is acquired by processing θ_r. The average error of $\hat{\theta}_r$ is reduced to ≈1° the maximums being about 3° or less. The corresponding $\hat{\omega}_{rm}$ plots in Fig. 6 exhibit a similar marginal error trend with the actual (ω_{rm}) and observed ($\hat{\omega}_{rm}$) velocity traces virtually overlapping over the entire speed range. Such performance outputs can be attributed to the majority of high-quality estimates being generated by the position estimator based on (10) and (13) which, together with the observer, works in a closed-loop fashion. Another contributing factor to the estimator robustness is the minimized sensitivity to L_p knowledge contingencies when $i_{sd} \approx 0$ and $\delta \approx -\pi/2$ in (13) according to Fig. 2.

The primary and secondary current components, ($i_{sd,q}$) and ($i_{pd,q}$), are presented in Fig. 8. The transient over-currents are avoided by the integrators of the PI controllers not having to

be saturated to attain the moderately varying command speeds. The desired MTPIA reference trajectory ($i^*_{sd} = 0$) is properly followed, while the i_{pd} is required to establish the machine flux by satisfying the specific Q demand stipulated by (7). A close resemblance in shape between the magnetizing i_{pd} and Q waveforms on one hand, and $i_{sq} \sim i_{pq}$ and P counterparts on the other, is clearly visible. The i_{pd} profile is smooth and shows no apparent signs of distortion in response to the speed related variations of i_{sq} and i_{pq} by analogy to Q in Fig. 6.

Fig. 9 illustrates the step-wise PWM sector change of the modulated secondary voltage vector ($\underline{v}_s$) while riding through the synchronous speed from 950 to 550 rev/min. At sub-synchronous speeds, $\underline{v}_s$ rotates clockwise with the sector numbers descending, which comes from the opposite phase sequence of the secondary to the primary winding since $\omega_s < 0$ in (1). In super-synchronous speed mode, however, the direction of $\underline{v}_s$ rotation is reversed (i.e., anti-clockwise) as indicated by the ascending sector numbers for the same phase sequence of the windings when $\omega_s > 0$ in (1). Notice that $\underline{v}_s$ is stationary at synchronous speed (750 rev/min) and dc secondary currents, i.e., $\omega_s = 0$ in (1).

VIII. Conclusion

An original sensorless primary flux-oriented control scheme for the adjustable speed BDFRG has been proposed and successfully experimentally verified by the results presented for challenging wind turbine-alike variable loading conditions of the small machine prototype. The controller should work equally well in motoring mode for similar electric drives with narrow speed ranges (e.g., centrifugal pumps). The main properties of the algorithm, and the underlying rotor position and speed estimation technique, can be summarized as follows:

1) Applicability in the low secondary frequency region down to synchronous speed of the BDFRG(M) when the inverter-fed winding is dc. Such operation is generally hard to realize with back-emf based control of singly-excited machines.
2) The rotor position and speed are estimated on-line allowing one to adequately replace the encoder readings.
3) The injection of any special signals or peculiar inverter switching strategies are not required unlike with many other sensorless methods for more traditional machines including DFIG. This is particularly advantageous at a large scale level but comes at the price of generator parameter dependence.
4) The high instantaneous accuracy of the angular position and velocity estimates is achieved by means of a conventional Luenberger-style closed-loop load model based observer and the rotor position estimator where measurements of the grid-connected winding quantities at line frequency, secondary currents, and the dc link voltage are used for calculations.
5) The current feedback is provided directly, and without any information on the rotor or control frame position, suggesting the immunity to estimation errors. This improves the controller stability and quality of response.
6) The entire estimation process only requires the primary winding parameters (e.g., L_p, R_p) and the drive train inertia (J), with the L_m knowledge being additionally needed for current control. The parameter dependence gets weaker with increasing machine sizes and negligible R_p effects.
7) The high robustness of the whole control system to parameter deviations has been accomplished by meticulous tuning of the fixed PI gains. Adaptive mechanisms may have to be implemented for further performance optimizations and enhanced versatility of the controller.

This paper is expected to make a step forward in sensorless control research on the BDFRG. The possibility of eliminating a shaft position or speed sensor should strengthen further the BDFRG standing relative to the BDFIG companion in terms of reliability and maintenance costs as a viable brushless candidate for wind power applications.

References

[1] L. Xu, L. Zhen, and E. Kim, "Field-orientation control of a doubly excited brushless reluctance machine," *IEEE Trans. Ind. Appl.*, vol. 34, no. 1, pp. 148–155, Jan./Feb. 1998.
[2] M. G. Jovanovic, R. E. Betz, and J. Yu, "The use of doubly fed reluctance machines for large pumps and wind turbines," *IEEE Trans. Ind. Appl.*, vol. 38, pp. 1508–1516, Nov./Dec. 2002.
[3] D. G. Dorrell and M. JovanoviM. Jovanovi, "On the possibilities of using a brushless doubly-fed reluctance generator in a 2 MW wind turbine," in *Proc. IEEE Ind. Appl. Soc. Annu. Meeting*, Oct. 2008, pp. 1–8.
[4] T. Long, S. Shao, E. Abdi, R. McMahon, and S. Liu, "Asymmetrical low-voltage ride through of brushless doubly fed induction generators for the wind power generation," *IEEE Trans. Energy Convers.*, vol. 28, no. 3, pp. 502–511, Sep. 2013.
[5] S. Ademi and M. Jovanovic, "Control of emerging brushless doubly-fed reluctance wind turbine generators," in *Large Scale Renewable Power Generation* (Ser. Green Energy and Technology), J. Hossain and A. Mahmud, Eds. Berlin, Germany: Springer-Verlag, 2014, pp. 395–411.
[6] R. Cardenas, R. Pena, S. Alepuz, and G. Asher, "Overview of control systems for the operation of DFIGs in wind energy applications," *IEEE Trans. Ind. Electron.*, vol. 60, no. 7, pp. 2776–2798, Jul. 2013.
[7] A. Oraee, E. Abdi, and R. McMahon, "Converter rating optimisation for a brushless doubly fed induction generator," *IET Renew. Power Gener.*, vol. 9, no. 4, pp. 360–367, 2015.
[8] J. Carroll, A. McDonald, and D. McMillan, "Reliability comparison of wind turbines with DFIG and PMG drive trains," *IEEE Trans. Energy Convers.*, vol. 30, no. 2, pp. 663–670, Jun. 2015.
[9] F. Spinato, P. J. Tavner, G. J. W. van Bussel, and E. Koutoulakos, "Reliability of wind turbine subassemblies," *IET Renew. Power Gener.*, vol. 3, no. 4, pp. 387–401, Dec. 2009.
[10] E. Abdi, R. McMahon, P. Malliband, S. Shao, M. Mathekga, P. Tavner, S. Abdi, A. Oraee, T. Long, and M. Tatlow, "Performance analysis and testing of a 250 kW medium-speed brushless doubly-fed induction generator," *IET Renew. Power Gener.*, vol. 7, no. 6, pp. 631–638, Nov. 2013.
[11] S. Tohidi, P. Tavner, R. McMahon, H. Oraee, M. Zolghadri, S. Shao, and E. Abdi, "Low voltage ride-through of DFIG and brushless DFIG: Similarities and differences," *Elect. Power Syst. Res.*, vol. 110, pp. 64–72, May. 2014.
[12] G. Marques and D. Sousa, "Understanding the doubly fed induction generator during voltage dips," *IEEE Trans. Energy Convers.*, vol. 27, no. 2, pp. 421–431, Jun. 2012.
[13] H. Gorginpour, H. Oraee, and R. McMahon, "A novel modeling approach for design studies of brushless doubly fed induction generator based on magnetic equivalent circuit," *IEEE Trans. Energy Convers.*, vol. 28, no. 4, pp. 902–912, Dec. 2013.
[14] A. Knight, R. Betz, and D. Dorrell, "Design and analysis of brushless doubly fed reluctance machines," *IEEE Trans. Ind. Appl.*, vol. 49, no. 1, pp. 50–58, Jan./Feb. 2013.
[15] A. Oraee, E. Abdi, S. Abdi, R. McMahon, and P. Tavner, "Effects of rotor winding structure on the BDFM equivalent circuit parameters," *IEEE Trans. Energy Convers.*, vol. 30, no. 4, pp. 1660–1669, Dec. 2015.

[16] M. Ruviaro, F. Runcos, N. Sadowski, and I. Borges, "Analysis and test results of a brushless doubly fed induction machine with rotary transformer," *IEEE Trans. Ind. Electron.*, vol. 59, no. 6, pp. 2670–2677, Jun. 2012.
[17] F. Xiong and X. Wang, "Design of a low-harmonic-content wound rotor for the brushless doubly fed generator," *IEEE Trans. Energy Convers.*, vol. 29, no. 1, pp. 158–168, Mar. 2014.
[18] J. Hu, J. Zhu, and D. Dorrell, "A new control method of cascaded brushless doubly fed induction generators using direct power control," *IEEE Trans. Energy Convers.*, vol. 29, no. 3, pp. 771–779, Sep. 2014.
[19] X. Chen, Z. Wei, X. Gao, C. Ye, and X. Wang, "Research of voltage amplitude fluctuation and compensation for wound rotor brushless doubly-fed machine," *IEEE Trans. Energy Convers.*, vol. 30, no. 3, pp. 908–917, Sep. 2015.
[20] S. Khaliq, M. Modarres, T. Lipo, and B.-i. Kwon, "Design of novel axial flux dual stator doubly fed reluctance machine," *IEEE Trans. Magn.*, vol. 51, no. 11, pp. 1–4, Nov. 2015.
[21] F. Wang, F. Zhang, and L. Xu, "Parameter and performance comparison of doubly-fed brushless machine with cage and reluctance rotors," *IEEE Trans. Ind. Appl.*, vol. 38, no. 5, pp. 1237–1243, Sep./Oct. 2002.
[22] R. E. Betz and M. G. Jovanović, "Introduction to the space vector modelling of the brushless doubly-fed reluctance machine," *Elect. Power Comput. Syst.*, vol. 31, no. 8, pp. 729–755, 2003.
[23] M. Jovanović, "Sensored and sensorless speed control methods for brushless doubly fed reluctance motors," *IET Elect. Power Appl.*, vol. 3, no. 6, pp. 503–513, 2009.
[24] J. Poza, E. Oyarbide, I. Sarasola, and M. Rodriguez, "Vector control design and experimental evaluation for the brushless doubly fed machine," *IET Elect. Power Appl.*, vol. 3, no. 4, pp. 247–256, Jul. 2009.
[25] F. Barati, R. McMahon, S. Shao, E. Abdi, and H. Oraee, "Generalized vector control for brushless doubly fed machines with nested-loop rotor," *IEEE Trans. Ind. Electron.*, vol. 60, no. 6, pp. 2477–2485, Jun. 2013.
[26] R. Zhao, A. Zhang, Y. Ma, X. Wang, J. Yan, and Z. Ma, "The dynamic control of reactive power for the brushless doubly fed induction machine with indirect stator-quantities control scheme," *IEEE Trans. Power Electron.*, vol. 30, no. 9, pp. 5046–5057, Sep. 2015.
[27] S. Ademi and M. Jovanović, "High-efficiency control of brushless doubly-fed machines for wind turbines and pump drives," *Energy Convers. Manage.*, vol. 81, pp. 120–132, May. 2014.
[28] S. Ademi and M. Jovanović, "Vector control methods for brushless doubly fed reluctance machines," *IEEE Trans. Ind. Electron.*, vol. 62, no. 1, pp. 96–104, Jan. 2015.
[29] S. Ademi, M. Jovanović, and M. Hasan, "Control of brushless doubly-fed reluctance generators for wind energy conversion systems," *IEEE Trans. Energy Convers.*, vol. 30, no. 2, pp. 596–604, Jun. 2015.
[30] M. G. Jovanović, J. Yu, and E. Levi, "Encoderless direct torque controller for limited speed range applications of brushless doubly fed reluctance motors," *IEEE Trans. Ind. Appl.*, vol. 42, no. 3, pp. 712–722, May/Jun. 2006.
[31] H. Chaal and M. Jovanović, "Practical implementation of sensorless torque and reactive power control of doubly fed machines," *IEEE Trans. Ind. Electron.*, vol. 59, no. 6, pp. 2645–2653, Jun. 2012.
[32] H. Chaal and M. Jovanovic, "Power control of brushless doubly-fed reluctance drive and generator systems," *Renew. Energy*, vol. 37, no. 1, pp. 419–425, Jan. 2012.
[33] F. Valenciaga and P. F. Puleston, "Variable structure control of a wind energy conversion system based on a brushless doubly fed reluctance generator," *IEEE Trans. Energy Convers.*, vol. 22, no. 2, pp. 499–506, Jun. 2007.
[34] S. Ademi and M. Jovanovic, "Control of doubly-fed reluctance generators for wind power applications," *Renew. Energy*, vol. 85, pp. 171–180, Jan. 2016.
[35] L. Xu, E. Inoa, Y. Liu, and B. Guan, "A new high-frequency injection method for sensorless control of doubly fed induction machines," *IEEE Trans. Ind. Appl.*, vol. 48, no. 5, pp. 1556–1564, Sep. 2012.
[36] F. Castelli-Dezza, M. Iacchetti, and R. Perini, "An observer for sensorless DFIM drives based on the natural fifth harmonic of the line voltage, without stator current measurement," *IEEE Trans. Ind. Electron.*, vol. 60, no. 10, pp. 4301–4309, Oct. 2013.
[37] G. Marques, D. Sousa, and M. Iacchetti, "An open-loop sensorless slip position estimator of a DFIM based on air-gap active power calculations-sensitivity study," *IEEE Trans. Energy Convers.*, vol. 28, no. 4, pp. 959–968, Dec. 2013.
[38] M. Felice Iacchetti, G. Marques, R. Perini, and D. Sousa, "Stator inductance self-tuning in an air-gap-power-vector-based observer for the sensorless control of doubly fed induction machines," *IEEE Trans. Ind. Electron.*, vol. 61, no. 1, pp. 139–148, Jan. 2014.
[39] D. Diaz Reigosa, F. Briz, C. Blanco, and J. Guerrero, "Sensorless control of doubly fed induction generators based on stator high-frequency signal injection," *IEEE Trans. Ind. Appl.*, vol. 50, no. 5, pp. 3382–3391, Sep./Oct. 2014.
[40] S. Abdi, E. Abdi, A. Oraee, and R. McMahon, "Equivalent circuit parameters for large brushless doubly fed machines (BDFMs)," *IEEE Trans. Energy Convers.*, vol. 29, no. 3, pp. 706–715, Sep. 2014.
[41] B. Mwinyiwiwa, Y. Zhang, B. Shen, and B.-T. Ooi, "Rotor position phase-locked loop for decoupled P-Q control of DFIG for wind power generation," *IEEE Trans. Energy Convers.*, vol. 24, no. 3, pp. 758–765, Sep. 2009.
[42] R. Lorenz and K. Patten, "High-resolution velocity estimation for all-digital, ac servo drives," *IEEE Trans. Ind. Appl.*, vol. 27, no. 4, pp. 701–705, Jul./Aug. 1991.
[43] S. Yang and V. Ajjarapu, "A speed-adaptive reduced-order observer for sensorless vector control of doubly fed induction generator-based variable-speed wind turbines," *IEEE Trans. Energy Convers.*, vol. 25, no. 3, pp. 891–900, Sep. 2010.
[44] M. Pattnaik and D. Kastha, "Adaptive speed observer for a stand-alone doubly fed induction generator feeding nonlinear and unbalanced loads," *IEEE Trans. Energy Convers.*, vol. 27, no. 4, pp. 1018–1026, Dec. 2012.

Sul Ademi (M'12) received the B.Eng. and Ph.D. degrees in electrical and electronics engineering from Northumbria University, Newcastle upon Tyne, U.K., in 2011 and 2014, respectively.

He is currently a Research Associate with the Department of Electronic and Electrical Engineering, University of Strathclyde, Glasgow, U.K. His research interests include electric motor drives, wind energy conversion, control of doubly fed machines for variable speed applications, and high voltage dc transmission.

Milutin G. Jovanović (M'99–SM'05) received the Dipl.Eng and M.E.E. degrees from the University of Belgrade, Belgrade, Serbia, in 1987 and 1991, respectively, and the Ph.D. degree from the University of Newcastle, Callaghan, N.S.W., Australia, in 1997, all in electrical engineering.

He is currently an Associate Professor with the Faculty of Engineering and Environment, Northumbria University, Newcastle upon Tyne, U.K. He has published more than 130 journal and conference papers. His major interests and activities include the areas of reluctance machine drives and wind power generation.

Hamza Chaal, photograph and biography not available at the time of publication.

Wenping Cao (M'05–SM'11) received the B.Eng. degree in electrical engineering from Beijing Jiaotong University, Beijing, China, in 1991, and the Ph.D. degree in electrical machines and drives from the University of Nottingham, Nottingham, U.K., in 2004.

He is currently a Chair Professor of Electrical Power Engineering with Aston University, Birmingham, U.K., and is also a Marie Curie Fellow with the Massachusetts Institute of Technology, Cambridge, MA, USA. His research interests include fault analysis, condition monitoring, and control of electric machines and power electronics.

Dr. Cao is an Associate Editor for the IEEE TRANSACTIONS ON INDUSTRY APPLICATIONS, IEEE INDUSTRY APPLICATIONS MAGAZINE, and *IET Power Electronics*. He is also the Chief Editor for three special issues and one book, an Editor for the *Electric Power Components and Systems Journal,* and nine other international journals.